PHYSICAL REVIEW D **91,** 075007 (2015)

Looking for hints of a reconstructible seesaw model at the Large Hadron Collider

Gulab Bambhaniya,[1,*] Srubabati Goswami,[1,†] Subrata Khan,[1,‡] Partha Konar,[1,§] and Tanmoy Mondal[1,2,‖]

[1]*Physical Research Laboratory (PRL), Ahmedabad 380009, Gujarat, India*

[2]*Indian Institute of Technology, Gandhinagar, Ahmedabad 382424, Gujarat, India*

(Received 27 October 2014; revised manuscript received 17 March 2015; published 9 April 2015)

We study the production of heavy neutrinos at the Large Hadron Collider through the dominant s-channel production mode as well as the vector boson fusion process. We consider the TeV scale minimal linear seesaw model containing two heavy singlets with the opposite lepton number. This model is fully reconstructible from oscillation data apart from an overall normalization constant which can be constrained from the metastability of the electroweak vacuum and bounds coming from lepton flavor violation searches. The Dirac nature of heavy neutrinos in this model implies suppression of the conventional same-sign-dilepton signal at the Large Hadron Collider. We analyze the collider signatures with the trilepton final state and missing transverse energy as well as vector boson fusion type signals which are characterized by two additional forward tagged jets. Our investigation reveals that due to stringent constraints on light-heavy mixing coming from lepton flavor violation and metastability bounds, the model can be explored only for a light to moderate mass range of heavy neutrinos. We also note that in case of a positive signal, flavor counting of the final trilepton channel can give information about the mass hierarchy of the light neutrinos.

DOI: 10.1103/PhysRevD.91.075007 PACS numbers: 12.60.-i, 13.35.Hb, 13.85.Qk, 14.60.St

I. INTRODUCTION

The discovery of the Higgs boson at the Large Hadron Collider by both ATLAS [1] and CMS [2] Collaborations has put the Standard Model (SM) on a firm footing. However, no signal of physics beyond the Standard Model has been found so far at the LHC. On the other hand, convincing indications of physics beyond the Standard Model have already emerged from the phenomenon of neutrino oscillation observed in terrestrial experiments. These results have conclusively established that neutrinos have nonzero mass and flavor mixing. Oscillation data together with the cosmological bound on sum of neutrino masses ($\Sigma m_i < 0.23$ eV including the PLANCK data [3]) indicate that neutrino masses are much smaller as compared to the other fermions in the SM. Such small masses can be generated naturally by the seesaw mechanism. The origin of seesaw is the dimension 5 effective operator $\frac{c_5}{M} LLHH$, where $L(H)$ being the SM lepton (Higgs) doublet and c_5 is a dimensionless coupling, M is the mass scale at which the effective operator gets generated [4]. Such operators arise by integrating out heavy fields added to the SM Lagrangian and they violate the lepton number by two units. The smallness of the neutrino mass in these models is related to the scale of lepton number violation which is required to be very high $\sim\mathcal{O}(10^{15}$ GeV) to generate neutrino masses in the right ballpark. The most economical in terms of particle contents is the type-I seesaw in which heavy singlet right-handed neutrinos are added to the SM Lagrangian [5–9]. However, the natural seesaw scale is far beyond the reach of the LHC. To have signatures of seesaw models at the LHC, the heavy neutrino (N) mass needs to be $\sim\mathcal{O}$ (TeV). However, if one lowers the scale of the seesaw to TeV then it also requires much smaller neutrino Yukawa couplings ($\sim 10^{-6}$) to obtain correct light neutrino masses. Such small Yukawa couplings lead to suppression of the production of the heavy neutrinos in natural TeV scale type-I seesaw models. This leads to the question of whether it is possible to achieve both the requirements simultaneously, i.e. having TeV scale heavy neutrinos along with large Yukawa coupling leading to large light-heavy mixing. Such possibilities can be realized in some specific mass textures [10–18]. Other options include models with higher-dimensional operators arising due to the exchange of new particles belonging to larger representations [19–27], radiative mass generations [28–35], etc. One of the most popular options to generate TeV scale seesaw is through the inverse seesaw models in which one includes additional singlet states. These models were first proposed in the context of E(6) grand unified theories [36]. In these models the seesaw scale is decoupled from the scale of lepton number violation and the smallness of the neutrino mass originates from the small lepton number violating terms in the Lagrangian.

In the type-I seesaw model the heavy and light neutrinos are both Majorana particles. It is well known that the Majorana nature of neutrinos can be established by observing a positive signal in neutrinoless double beta

*gulab@prl.res.in
†sruba@prl.res.in
‡subrata@prl.res.in
§konar@prl.res.in
‖tanmoym@prl.res.in

decay experiments. It was noticed in [37], in the context of the left-right symmetric model that resonant production of N and its subsequent decay giving the same-sign-dilepton (SSDL) signal in colliders can also constitute evidence for the Majorana nature of neutrinos. Given the importance of this signal, there have been several studies of this channel at the hadron colliders [38–43] including searches at the LHC [44]. Enhanced contribution from the infrared t-channel, especially for heavier masses, was proposed [45,46] together with s-channel production.

The heavy neutrinos in the inverse seesaw model are of the pseudo-Dirac nature and in this case the SSDL signal is suppressed by the small lepton number violating coupling. For such models the heavy neutrinos are produced by the s-channel process along with a charged lepton. This neutrino further decays to a second lepton (of sign opposite to the first lepton to conserve the lepton number) together with a W-boson. The W-boson can further decay leptonically to produce a lepton and a neutrino. Thus, the final signal consists of trilepton and missing energy which is expected to have a tiny contamination from the Standard Model backgrounds. Detailed studies including the SM background in the context of pseudo-Dirac neutrinos have been done in [42,47]. Similar studies in the context of the left-right symmetric model, nonminimal supersymmetric inverse seesaw models, and the type-III seesaw model have been performed in [48,49], and [50], respectively. Experimental searches for multilepton signals have been carried out by the CMS Collaboration using an integrated luminosity of 19.5 fb^{-1} with center of mass energy $\sqrt{s} =$ 8 TeV at the LHC [51]. They considered at least three leptons in the final state using a search strategy not specific to any particular model.

In this work, we consider the minimal linear seesaw model (MLSM) studied in [52,53] as an example of the TeV scale seesaw model. This is a variant of the inverse seesaw model but in this case the minimal scheme consists of adding just two heavy singlets with the opposite lepton number as opposed to four heavy neutrinos in canonical minimal inverse seesaw models [54]. It was shown in [52] that the Yukawa coupling matrices for this model can be fully reconstructed in terms of the oscillation parameters apart from an overall normalization factor. It was further shown in [53] that this normalization constant can be constrained from consideration of the metastability of the electroweak vacuum and lepton flavor violation bounds. The heavy neutrinos in this model are of Dirac type and the SSDL signal is suppressed.[1] In the context of this model, we consider two possible production channels for the heavy neutrinos resulting in two different classes of signals. The first one of this is the s-channel process to produce heavy Dirac neutrinos associated with a lepton and finally giving the trilepton and missing energy signal. The second one is the production of heavy neutrinos through vector boson fusion (VBF) in which two electroweak vector bosons coming from two partons "fuse" to produce the signal under consideration (trileptons) along with two highly forward jets. It becomes important in the context of hadron colliders since the tagging of forward jets allows us to reduce the background considerably. Also the lack of color exchange between these jets makes the central region free from the color activities and this is exploited by vetoing central jets; see [55] and references therein in the context of the Higgs search. This helps in minimizing the backgrounds further. For these reasons VBF remains an important channel to look for new physics [56–58] at hadron colliders.

We consider both normal hierarchy (NH) as well as inverted hierarchy (IH) for the light neutrino mass spectra. We also estimate the corresponding Standard Model backgrounds for the 14 TeV LHC. In each case, we perform a realistic simulation with extensive event selections using MadGraph and PYTHIA.

The paper is organized as follows: Sec. II contains a brief description of the model. The production and decay of the right-handed neutrino at the LHC are discussed in Sec. III. Simulation details and results are presented in Sec. IV, while in Sec. V we discuss the discovery potential of the signals at the LHC. Finally, we conclude in Sec. VI.

II. THE LINEAR SEESAW MODEL

The most general Lagrangian containing heavy singlet fields N_R and S with opposite lepton numbers is given by

$$-\mathcal{L} = \bar{N}_R Y_\nu \tilde{\phi}^\dagger l_L + \bar{S} Y_S \tilde{\phi}^\dagger l_L + \bar{S} M_N N_R^c + \frac{1}{2}\bar{S}\mu S^c + \frac{1}{2}\overline{N_R}\mu_N N_R^c + \text{H.c.}, \tag{1}$$

where $l_L = (\nu_x, x)_L^T$, $x = e, \mu, \tau$.

Once the symmetry is broken spontaneously, the Higgs field ϕ obtains a vacuum expectation value equal to $v/\sqrt{2}$. This generates the Dirac mass term $m_D = Y_\nu v/\sqrt{2}$ and the lepton number breaking mass term $m_S = Y_S v/\sqrt{2}$. In the linear seesaw models [59–61] one assumes m_S to be small and nonzero while the μ and the μ_N terms are set to zero. This can be done since they contribute towards the light neutrino mass in the subleading orders [62]. Since lepton number violating mass terms are set to zero, the heavy neutrinos are purely Dirac type. Then the mass matrix takes the form

$$\mathcal{M}_\nu = \begin{pmatrix} 0 & m_D^T & m_S^T \\ m_D & 0 & M_N \\ m_S & M_N^T & 0 \end{pmatrix}, \tag{2}$$

in the (ν_L, N_R^c, S^c) basis.

[1] Because of the same reason the heavy neutrino contribution towards $0\nu\beta\beta$ is suppressed [53].

TABLE I. Allowed 3σ ranges of oscillation parameters and benchmark values of these parameters used in our analysis to get the signal allowed by LFV and vacuum metastability. Case I corresponds to the peak in Fig. 1 (left panel), while case II corresponds to a lower value of y_ν/M_N, for which $V_{\mu N}$ is maximum. The value of the Majorana phase α is set at $3\pi/2(3\pi/4)$ for the NH (IH) scenario.

	Parameter					
Bound	$\Delta^2_\odot[10^{-5}\ \mathrm{eV}^2]$	$\Delta^2_{\mathrm{atm}}[10^{-3}\ \mathrm{eV}^2]$	$\sin^2\theta_{12}$	$\sin^2\theta_{23}$	$\sin^2\theta_{13}$	δ
3σ range (NH)	7.12–8.20	2.31–2.74	0.27–0.37	0.36–0.68	0.017–0.033	0–2π
(IH)		2.21–2.64		0.37–0.67		
Used value (NH: case I)	7.15	2.73	0.27	0.36	0.033	0.0
Used value (NH: case II)	7.13	2.73	0.27	0.68	0.033	0.0
Used value (IH)	7.25	2.40	0.34	0.57	0.021	0.0

The minimal model which can successfully generate two light neutrinos with nonzero mass is when only two extra heavy singlets are added to the SM Lagrangian. This is called the MLSM [52,53]. The full mass matrix has dimension 5×5 and can be written as

$$\mathcal{M}_\nu = \begin{pmatrix} 0 & m_D'^{\,T} \\ m_D' & M \end{pmatrix}, \tag{3}$$

where $m_D'^T = (m_D^T, m_S^T)$ and

$$M = \begin{pmatrix} 0 & M_N \\ M_N & 0 \end{pmatrix}. \tag{4}$$

For the minimal case, M_N is just a number, not a matrix. $\mathcal{M}_\nu$ can be diagonalized by a 5×5 unitary matrix U_0 as

$$U_0^T \mathcal{M}_\nu U_0 = \mathcal{M}_\nu^{\mathrm{diag}}, \tag{5}$$

where $\mathcal{M}_\nu^{\mathrm{diag}} = \mathrm{diag}(m_1, m_2, m_3, M_1, M_2)$. Following a two-step diagonalization procedure [63], U_0 can be expressed as

$$U_0 = \begin{pmatrix} (1-\frac{1}{2}\epsilon)U_\nu & m_D^\dagger (M^{-1})^* U_R \\ -M^{-1} m_D U_\nu & (1-\frac{1}{2}\epsilon')U_R \end{pmatrix} \equiv \begin{pmatrix} U_L & V \\ S & U_H \end{pmatrix}, \tag{6}$$

where U_L is the U_{PMNS} mixing matrix, and V, S are the light-heavy mixing matrices. Interaction of heavy neutrinos with the SM fields is determined by the mixing matrix V, whose elements will be denoted as V_{lN} hereafter. We would notice afterwards that the strong constraints on some elements of this matrix, i.e. V_{eN} and $V_{\mu N}$, would restrict the production signal. The diagonalizing matrix is now nonunitary which is characterized by the factor $(1-\epsilon/2)$. The nonunitary corrections ϵ and ϵ' are given in [63,64]. U_ν is the unitary component of U_{PMNS} which is same as U_{PMNS} for $\epsilon \ll 1$. We use the standard parametrization for this:

$$U_\nu = \begin{pmatrix} c_{12}c_{13} & s_{12}c_{13} & s_{13}e^{-i\delta} \\ -c_{23}s_{12} - s_{23}s_{13}c_{12}e^{i\delta} & c_{23}c_{12} - s_{23}s_{13}s_{12}e^{i\delta} & s_{23}c_{13} \\ s_{23}s_{12} - c_{23}s_{13}c_{12}e^{i\delta} & -s_{23}c_{12} - c_{23}s_{13}s_{12}e^{i\delta} & c_{23}c_{13} \end{pmatrix} P, \tag{7}$$

where $c_{ij} = \cos\theta_{ij}$, $s_{ij} = \sin\theta_{ij}$, and δ denotes the Dirac CP phase. The Majorana phase matrix P is expressed as $P = \mathrm{diag}(e^{-i\alpha}, e^{i\alpha}, 1)$; there is only one Majorana phase because one of the mass eigenvalues is zero. In Table I, we have presented the 3σ allowed range of oscillation parameters. Note that the phases are completely unconstrained at present.

Using the seesaw approximation, one obtains the light neutrino mass matrix,

$$m_{\mathrm{light}} = m_D'^T M^{-1} m_D'. \tag{8}$$

This being a rank 2 matrix, the light neutrinos belonging to this model are hierarchical. Thus, there are two possible mass spectra:

(i) NH: $(m_1 < m_2 < m_3)$
(ii) IH: $(m_3 \ll m_2 \approx m_1)$.

In the MLSM, Y_ν and Y_S are 3×1 matrices [cf. Eq. (1)] and can be considered as two independent vectors

$$Y_\nu \equiv y_\nu \hat{\mathbf{a}}; \qquad Y_S \equiv y_s \hat{\mathbf{b}}, \tag{9}$$

where $\hat{\mathbf{a}}$ and $\hat{\mathbf{b}}$ denote complex vectors with unit norm while y_ν and y_s represent the norms of the Yukawa matrices Y_ν and Y_S, respectively. Using Eqs. (8) and (9) one can reconstruct the Yukawa matrices Y_ν and Y_S in terms of the oscillation parameters barring an overall normalization factor. The parametrization of the Yukawa matrices depends on the mass hierarchy and can be expressed as [52,53]

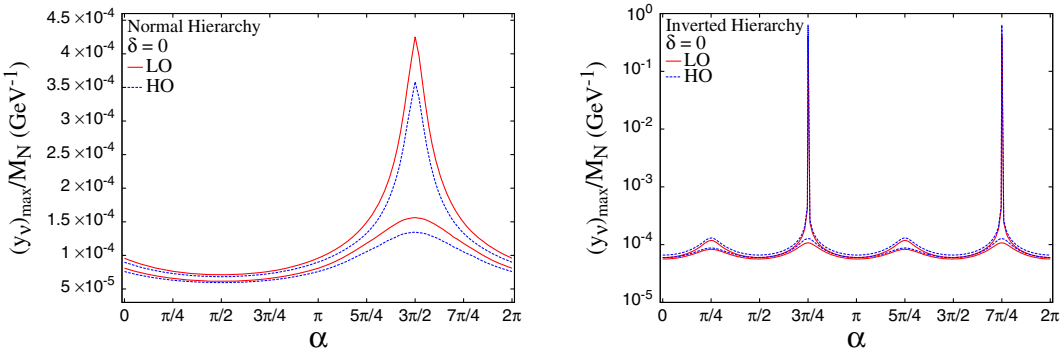

FIG. 1 (color online). Bound on y_ν/M_N as a function of the Majorana phase α, varying the oscillation parameters in the allowed 3σ range. The red-solid (blue-dashed) curve corresponds to the atmospheric angle (θ_{23}) residing in the LO (HO) region. (Left plot) The plot is for the NH scenario, where the highest allowed value of y_ν/M_N lies in the LO region. (Right plot) The same plot for the IH scenario.

$$Y_\nu = \frac{y_\nu}{\sqrt{2}}\left(\sqrt{1+\rho}U_j^\dagger + e^{i\frac{\pi}{2}}\sqrt{1-\rho}U_k^\dagger\right),$$
$$Y_S = \frac{y_s}{\sqrt{2}}\left(\sqrt{1+\rho}U_j^\dagger - e^{i\frac{\pi}{2}}\sqrt{1-\rho}U_k^\dagger\right), \qquad (10)$$

where $j=2$, $k=3$ for NH and $j=2$, $k=1$ for IH. U_j's denote the columns of the unitary matrix U_ν that diagonalizes the light neutrino mass matrix $m_{\rm light}$ in Eq. (8). The parameter ρ is given as

$$\rho = \frac{\sqrt{1+r}-\sqrt{r}}{\sqrt{1+r}+\sqrt{r}}({\rm NH}), \qquad \rho = \frac{\sqrt{1+r}-1}{\sqrt{1+r}+1}({\rm IH}). \quad (11)$$

Here r denotes the ratio of the solar and atmospheric mass squared differences, $r = \Delta m^2_\odot/\Delta m^2_{\rm atm}$, with $\Delta m^2_\odot \equiv m_2^2 - m_1^2$ and $\Delta m^2_{\rm atm} \simeq m_3^2 - m_1^2 (m_2^2 - m_3^2)$ for NH (IH).

The overall coupling y_ν can be constrained from the metastability of the electroweak vacuum and LFV [53]. For NH the most stringent constraint comes from LFV, whereas for the IH case the vacuum metastability constraint is more restrictive. This is because of cancellations occurring for the IH for LFV processes [53]. The dependence of the bound on y_ν from metastability and LFV on the heavy neutrino mass has been shown in [53]. The metastability bound on y_ν varies approximately in the range 0.4–0.5 for M_N varying in the range 100–1000 GeV. This bound is independent of the oscillation parameters. However, significant variation on the bound on y_ν from the LFV constraint is possible within the allowed range of oscillation parameters, mostly due to unconstrained phases, δ and α. Details of these dependences can be followed from Fig. 1. For a particular M_N, the strength of the signal at the LHC would depend on the value of y_ν. To maximize the signal, we therefore choose the value of y_ν at the peak for the NH case. However, for the IH case the peak value is much above the vacuum metastability bound and therefore we choose the maximum allowed value of y_ν satisfying the metastability bound. The corresponding parameter values are depicted in Table I for NH (case I) and IH. Note that, the above mentioned cancellations within the terms, ensure the peak position corresponds to $\alpha+\delta = 3\pi/2(3\pi/4)$ for NH (IH), which is also evident in Fig. 1. We have chosen $\delta = 0$ in our analysis. For some other values of δ, the phase α has to be chosen so that one is at the peak. In Fig. 1 we also show the variation of this bound with respect to the θ_{23} mixing angle in the lower octant (LO, $\theta_{23} < \pi/4$) and higher octant (HO, $\theta_{23} > \pi/4$). The y_ν value 0.4 (0.075) corresponds to the IH (NH: case I) scenario for $M_N = 100$ GeV, which we will use in our analysis. These will be translated into the bounds on the mixing matrix elements, V_{lN}, depending on the heavy neutrino mass M_N. Since y_s is extremely small [$\mathcal{O}(10^{-10})$], Y_S does not play any role in determining V_{lN}. The elements of the matrix V(or V_{lN}) can be expressed in terms of the $U_{\rm PMNS}$ matrix, ρ and y_ν as follows:

$$\begin{aligned}
V_{eN_1} &= \frac{-i}{\sqrt{2}M_N}\frac{y_\nu v}{2}[\sqrt{1+\rho}(U_{\rm PMNS})^*_{12} + i\sqrt{1-\rho}(U_{\rm PMNS})^*_{11}] \\
&\simeq \frac{y_\nu v}{4M_N}[e^{i(\alpha+\delta)}(-2+\sqrt{r})r^{\frac{1}{4}}s_{12} - 2i\,s_{13}] + \mathcal{O}((\sqrt{r}, s_{13})^2) \\
V_{\mu N_1} &= \frac{-i}{\sqrt{2}M_N}\frac{y_\nu\, v}{2}(\sqrt{1+\rho}(U_{\rm PMNS})^*_{22} + i\sqrt{1-\rho}(U_{\rm PMNS})^*_{21}) \\
&\simeq \frac{y_\nu\, v}{4M_N}[(-2+\sqrt{r})(e^{i\alpha}r^{\frac{1}{4}}c_{12}c_{23} + i\,s_{23}) + 2e^{i(\alpha+\delta)}r^{\frac{1}{4}}s_{12}s_{23}s_{13}] + \mathcal{O}((\sqrt{r}, s_{13})^2). \qquad (12)
\end{aligned}$$

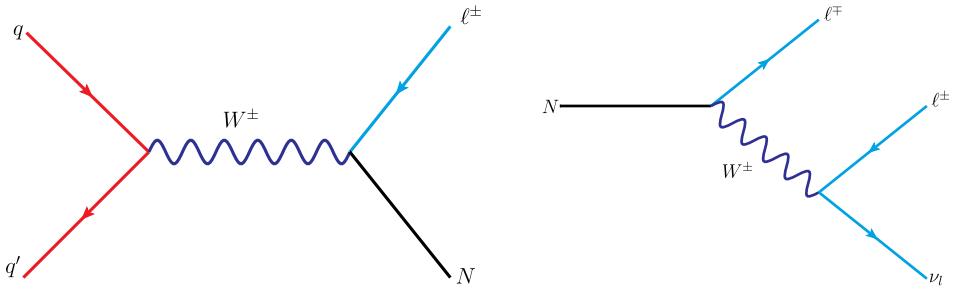

FIG. 2 (color online). (Left plot) Leading order s-channel diagram for heavy neutrino production at hadron colliders, and (right plot) representative diagram for one of the decay modes of the heavy neutrino. These two figures lead to the trilepton $+\not{E}_T$ signal considered in the analysis.

The above expressions are for the NH scenario and similar expressions can be computed for IH also. The element V_{eN_2} $(V_{\mu N_2})$ differs from $V_{eN_1}(V_{\mu N_1})$ by a phase factor. Note that in Table I, we also consider a second set of oscillation parameters for NH (NH: case II) corresponding to a lower value of y_ν of 0.056 with θ_{23} in the higher octant. This value is chosen such that $V_{\mu N}$ is the maximum and the muon signal may be larger, since the muon has higher efficiency for detection.

To get some perspective on the degree of suppression in the cross section coming from these constraints, we note down the corresponding V_{lN} values for $M_N = 100$ GeV as $V_{eN} = 1.95 \times 10^{-3}$, $V_{\mu N} = 2.93 \times 10^{-2}$, and $V_{\tau N} = 8.83 \times 10^{-2}$ for the NH (case I) scenario, whereas, $V_{eN} = 1.43 \times 10^{-3}$, $V_{\mu N} = 4.14 \times 10^{-2}$, and $V_{\tau N} = 5.48 \times 10^{-2}$ for the NH (case II), respectively. For IH these values are $V_{eN} = 0.48$, $V_{\mu N} = 4.15 \times 10^{-9}$, and $V_{\tau N} = 0.109$. Note that since our model is fully reconstructible and the only unknown parameter is y_ν, which can be constrained from LFV and metastabilty bounds, we have definite predictions for the parameters V_{lN} and these values are different for NH and IH scenarios. Bounds on V_{lN} can also come from electroweak precision data [65]. Our bounds for NH are consistent with these bounds. For IH we get a larger value for V_{eN}. However, it is to be noted that the electroweak precision data bounds are obtained assuming mixing with a single charged lepton and can be evaded in the presence of cancellations or mixing with the other charged leptons [42].

III. PHENOMENOLOGY AT THE LHC

The dominant production channel of the heavy neutrinos at the LHC is the s-channel process through virtual W-boson exchange. At the leading order the parton level process ($q\bar{q}' \to W^\pm \to \ell^\pm N$) is depicted in Fig. 2 (left plot). The heavy neutrinos can also be produced through the VBF process where production of N is associated with two forward jets. Figure 3 contains the representative parton level Feynman diagrams for VBF processes.[2] Estimated total production cross sections of these heavy Dirac neutrinos at the 14 TeV LHC in the IH scenario are shown in Fig. 4 for both s-channel (solid-line) as well as VBF (dashed-line). For the NH scenario the s-channel production cross sections are shown in the same figure for two different cases (cf. Table I), case I (red dot-dashed line) and case II (black double dotted line). Basic cuts such as $p_{T\ell} > 20$ GeV and $|\eta_\ell| < 2.5$ are applied and y_ν values mentioned in the previous section are used. It is seen from the figure that although case II corresponds to a lower value of y_ν since $V_{\mu N}$ is larger, the production cross section is slightly larger. Since the VBF cross section is much lower, we do not present the VBF cross section for the NH case. In these analyses CTEQ6L1 [68], parton distribution functions have been used with the factorization scale set at the heavy neutrino mass M_N.

Heavy neutrinos N can decay into charged leptons or neutrinos associated with the gauge (or Higgs) boson.

$$N \to W^\pm l^\mp / Z\nu_l / H\nu_l, \quad \text{where } l \equiv e, \mu, \tau. \tag{13}$$

A representative diagram for the decay of N ($N \to \ell^\mp W^\pm$) is shown in Fig. 2 (right plot).

In Fig. 5 we present the branching ratios (BRs) for these decay channels as a function of heavy neutrino mass M_N both in the case of normal hierarchy (left) and inverted hierarchy (right). Total decay widths in each case are also demonstrated with the solid line in each figure. Identifying that the charged lepton decay modes for the heavy neutrino, i.e. $N \to W^\pm l^\mp$ are the main channel for the search at the hadron collider, we discuss the corresponding decay modes in detail for both scenarios. The figure clearly shows that for NH,

[2]Note that there are some diagrams which are not truly the VBF type, i.e. two gauge boson are not fused via the t-channel (e.g. bottom right diagram in Fig. 3), but they can lead to the same final states. These diagrams are necessary for the requirements of gauge invariance and included both for background [66,67] and signal calculations.

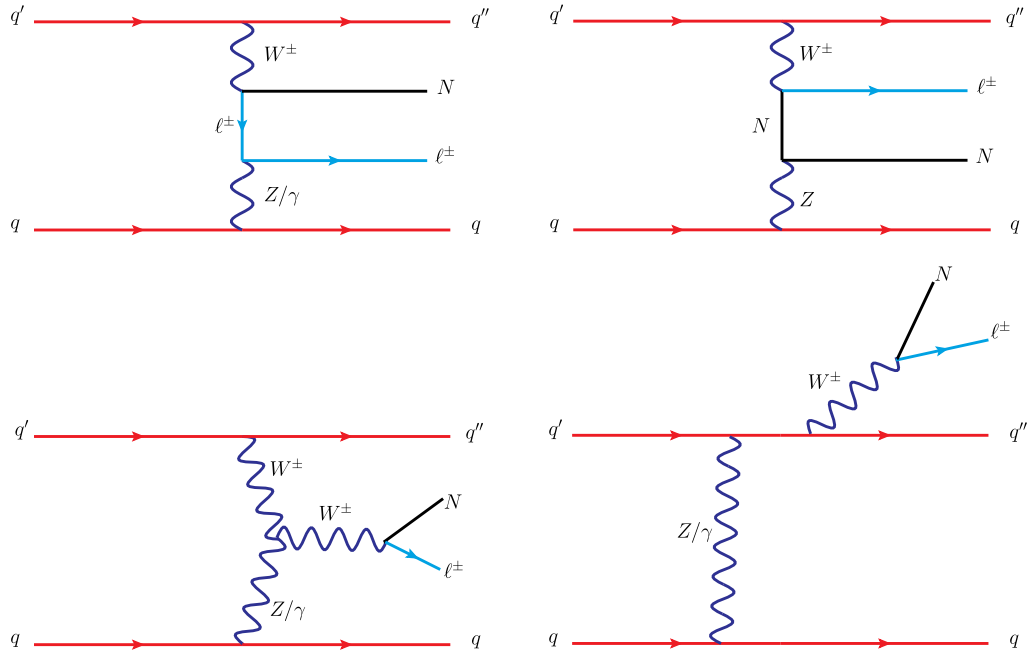

FIG. 3 (color online). Representative parton level diagrams contributing to $N\ell jj$ production through vector boson fusion at hadron colliders. Mirror diagrams are not shown here and also the last diagram is one of the four diagrams with $W^\pm$ emitting from each of the quark legs.

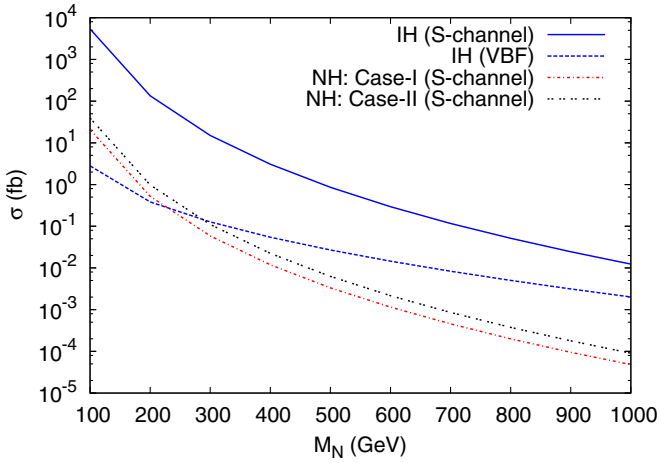

FIG. 4 (color online). The total cross section is shown for the production of the heavy neutrino associated with the light lepton ($pp \to N\ell$, where $\ell = e, \mu$) at the 14 TeV LHC through the leading order s-channel process, while dotted lines represent VBF production cross section.

case I,[3] heavy neutrinos mostly decay into the tau lepton (τ) and W-boson. On the other hand for IH, decay into the first generation lepton (e) possesses the maximum branching ratio. For NH the decay to μ is low and decay to e is severely suppressed, while for IH, the decay to τ has a lower ratio and decay to μ is negligible. The $W^\pm$ can have hadronic decay modes ($W^\pm \to jj$) or leptonic decay modes ($W^\pm \to l^\pm\nu$). The trilepton signal $pp \to l^\pm l^\mp l^\pm \nu$ comes from the later decay mode.[4]

Other than the charged lepton decay mode, N can also decay to the Z-boson or Higgs boson associated with the neutrinos as listed in Eq. (13). The corresponding branching ratios are also shown in Fig. 5. Note that the branching ratio for $Z\nu$ is suppressed for lower values of the masses of the heavy neutrinos essentially because of the W mass threshold. For the $H\nu$ decay mode, the Higgs mass threshold suppresses the decay rate for lower values of $M_N \sim 100$ GeV. However, as M_N increases, these branching ratios increase to retain a ~25% level. Both these channels can contribute to the trilepton signal via leptonic decays and we have considered their contributions in our simulation. However, since we will apply the Z-veto (to minimize the SM background), the contribution coming

[3]For case II, although branching ratios to different channels are likely to change, we do not show the corresponding plot as the final production cross section for both the cases, after putting all the selection criteria, is very low for NH and beyond the reach of the LHC at 14 TeV even with a luminosity of 3000 fb^{-1}.

[4]Evidently, the former decay mode leads to opposite sign dileptons (OSDL), also suppressed by $|V_{lN}|^4$, but slightly larger compare to the trilepton signal. However, significant irreducible backgrounds can come from $t\bar{t}$, VV (with $V = W, Z$), as well as Z + Jets after vetoing the dilepton invariant mass at Z-pole. Hence, we are not considering the OSDL as a signal. An estimate of these backgrounds for OSDL can be found in [69]. Note that their more specific selection criteria are not applicable for our present signal. Similarly, OSDL through VBF is suppressed by $|V_{lN}|^4$ and is beset with a large background coming from WW, $\tau\tau$, and ZZ production at VBF [57].

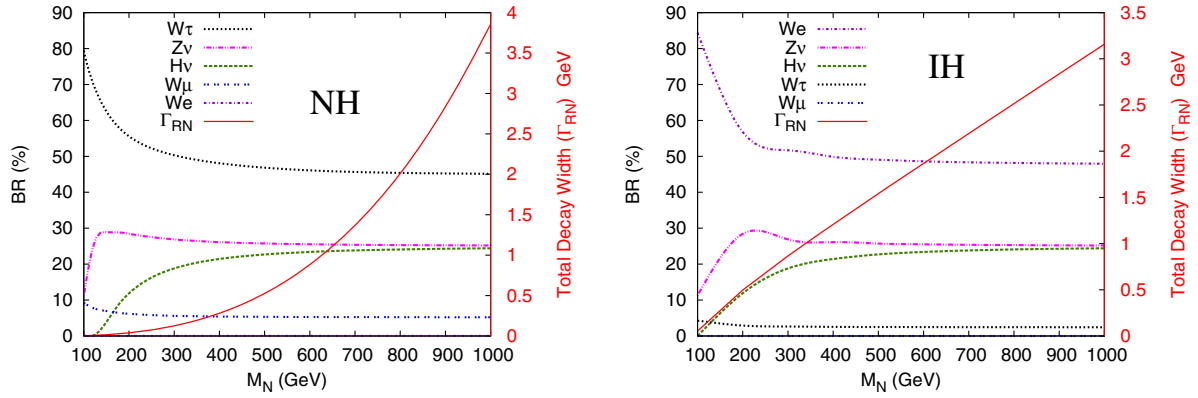

FIG. 5 (color online). The decay branching ratios of the heavy neutrino (N) in different channels as a function of its mass in the case of normal hierarchy, case I, (left) and inverted hierarchy (right). Total decay widths in each case are also demonstrated with the solid line in the same figure.

from the $Z\nu$ decay mode will be suppressed after final event selection.

As the lepton Yukawa is small, the $H\nu$ mode is also not going to contribute to our signal even for higher values of M_N.

IV. SIMULATION AND RESULTS

We have implemented the model in FeynRules [70] and generated the Feynman rules compatible with MadGraph5 [71]. After generating the Les Houches Event [72] file from MadGraph, we have passed that to PYTHIA6 [73] for showering and hadronization.

A. Selection criteria

To get enhancement in signal over background, we use the following selection criteria [74,75]:

(1) Identification criteria of a lepton: Pseudorapidity $|\eta_\ell| < 2.5$ and $p_{T\ell} > 20$ GeV have been used.
(2) Detector efficiency for leptons [76,77]:
  (a) For the electron (either e^- or e^+), detector efficiency is 0.7 (70%);
  (b) For the muon (either μ^- or μ^+), detector efficiency is 0.9 (90%).
(3) Smearing[5] of electron energy and muon p_T are incorporated.
(4) Lepton-lepton separation: For this, $\Delta R_{ll} \geq 0.2$ is used[6] (due to the detector resolution of leptons).
(5) Lepton-photon separation: This is taken as $\Delta R_{l\gamma} \geq 0.2$ with all the photons having $p_{T\gamma} > 10$ GeV.
(6) Lepton-jet separation: The separation of a lepton with all the jets is set at $\Delta R_{lj} \geq 0.4$; otherwise that lepton is not counted as a lepton. Jets are constructed from hadrons using PYCELL within the PYTHIA.
(7) Hadronic activity cut: This cut is applied to take only the pure kind of leptons that have very less hadronic activity around them. The hadronic activity within the cone of radius 0.2 around the lepton should be small, $\frac{\sum p_{T_{\rm hadron}}}{p_{T_l}} \leq 0.2$.
(8) Hard p_T cuts used are $p_{Tl_1} > 30$ GeV, $p_{Tl_2} > 30$ GeV, and $p_{Tl_3} > 20$ GeV.
(9) Missing p_T cut: Because of the presence of the neutrino, a missing p_T cut (> 30 GeV) is applied.
(10) Z-veto[7] is applied to suppress the SM background.
(11) VBF cuts [55,78]:
  (a) Central jet veto is also applied, in which we consider any jet with $E_{T3} > 20$ GeV and compute the rapidity with respect to the average of the two forward jets: $\eta_0 = \eta_3 - (\eta_1 + \eta_2)/2$. We veto the event if $|\eta_0| < 2$. The central jet veto is applied to suppress the QCD background substantially.
  (b) Charged leptons need to fall in between the rapidities of two forward tagging jets, i.e. $\eta_{j,\rm min} < \eta_\ell < \eta_{j,\rm max}$.
  (c) p_T of jets: $p_{Tj_1,j_2} > 20$ GeV.
  (d) Invariant mass of jets: $M_{j_1 j_2} > 600$ GeV.
  (e) Pseudorapidity of jets: $\eta_{j_1}.\eta_{j_2} < 0$ and $|\eta_{j_1} - \eta_{j_2}| > 4$. Demanding both the tagged jets in the opposite hemisphere and a large rapidity separation among them significantly reduces the background for VBF.

[5]The choice of corresponding η dependent parameters is similar to one of our earlier work [74].

[6]Here $\Delta R_{ij} = \sqrt{(\eta_i - \eta_j)^2 - (\phi_i - \phi_j)^2}$ quantifies the separation between particles i and j in the pseudorapidity (η)-azimuth (ϕ) plane.

[7]The same flavored but opposite sign lepton pair invariant mass $m_{\ell_1\ell_2}$ must be sufficiently away from the Z mass, such that, typically, $|m_{\ell_1\ell_2} - M_Z| \geq 6\Gamma_Z \sim 15$ GeV.

TABLE II. Dominant Standard Model background cross sections contributing to trilepton and missing transverse energy. These are calculated satisfying all the cuts (except VBF cuts) for the 14 TeV LHC. For each process we also classify the trilepton background into four different flavor combinations and present the cross section in each case along with the total contribution.

	Cross section (fb)				
Process	$\ell\ell\ell$	eee	$ee\mu$	$e\mu\mu$	$\mu\mu\mu$
$t\bar{t}$	18.972	1.1383	7.0831	8.2214	2.5297
$W^{\pm}(Z/\gamma^*)$	10.832	0.0677	0.1311	5.9891	4.6440
$(Z/\gamma^*)(Z/\gamma^*)$	1.175	0.0734	0.0525	0.6400	0.4090
$t\bar{t}(Z/\gamma^*)$	1.103	0.0429	0.1329	0.4997	0.4275
$t\bar{t}W^{\pm}$	0.639	0.0328	0.2655	0.2424	0.0983
TOTAL	**32.721**	**1.3551**	**7.6651**	**15.5926**	**8.1085**

TABLE III. Dominant Standard Model background cross section contributing to the trilepton and missing transverse energy associated with two forward jets. These are calculated satisfying all the cuts including VBF cuts for the 14 TeV LHC. Cross sections of four different flavor combinations as well as the total cross section are listed.

	Cross section (fb)				
Process	$\ell\ell\ell$	eee	$ee\mu$	$e\mu\mu$	$\mu\mu\mu$
W^+Zjj	0.04068	0.00073	0.00105	0.02157	0.01734
W^-Zjj	0.01923	0.00038	0.00055	0.00994	0.00836
$ZZjj$	0.00094	0.00002	0.00002	0.00066	0.00024
TOTAL	**0.06085**	**0.00113**	**0.00162**	**0.03216**	**0.02594**

B. Background

1. For the s-channel signal

To calculate the SM background we consider all channels that can produce or mimic the trilepton production with missing P_T. We closely follow the reference [74,79] where a similar background analysis was done with the event selection criteria listed as above except the cuts related to the VBF. Events are generated using ALPHGEN [80] for the processes coming from $t\bar{t}$, $t\bar{t}(Z/\gamma^*)$, $t\bar{t}W^{\pm}$, $W^{\pm}(Z/\gamma^*)$, $(Z/\gamma^*)(Z/\gamma^*)$ at the parton level and passed into PYTHIA. As expected $t\bar{t}$ and $W^{\pm}(Z/\gamma^*)$ contribute dominantly. These and other SM backgrounds are listed in Table II. For each process, we classify the trilepton signals into four different flavor combinations and compute the cross section in each case along with the total contribution.

2. For VBF signal

The trilepton signal with missing P_T and two forward jets in VBF can be faked by different SM backgrounds. Processes like $t\bar{t}$ would produce b-jets and are mostly effective in the central region. Vetoing on jet activities in the central region can eliminate most of the non-VBF type SM processes. However, the most important irreducible background comes from $W^{\pm}Z$ and ZZ together with two extra forward jets once the gauge bosons decay leptonically. These processes can construct a dominant SM background for the VBF production of $3\ell + E_T$ since they includes the typical VBF topology and hence can easily pass the central jet veto criteria. These backgrounds are calculated[8] using MadGraph5 and PYTHIA6. In Table III the dominant background cross sections, after satisfying all the cuts including VBF cuts at 14 TeV LHC, are tabulated. Like the case of s-channel backgrounds, for each process we also classify the trilepton signals into four different flavor combinations and compute the cross section in each case as well as the total contribution.

C. Signal

Earlier in Sec. III we have presented the total heavy neutrino production cross sections for different light neutrino hierarchies with basic selection criteria. The cross section for the NH scenario was found to be much lower than the IH scenario for the s-channel. The branching ratios for decays of N to final states with μ and e are also very small for NH. Therefore, we will concentrate only on the IH scenario henceforth. For this we consider both s-channel and VBF process. Although the VBF cross section for IH is lower or comparable to the s-channel cross section for NH for lower values of M_N, the background for VBF processes are much smaller. Hence, we study this channel also for IH. In this section we consider all leptonic decay modes of

[8]Next to leading order QCD corrections are available in [66,67].

TABLE IV. Cross section for the IH case. Final trilepton signal cross section through s-channel heavy neutrino production at the 14 TeV LHC for the benchmark point $M_N = 100$ GeV including all event selection cuts except VBF cuts. We classify the trilepton signals into four different flavor combinations and present the cross section in each case along with the total light lepton contribution.

	Cross section (fb)				
Hierarchy	$\ell\ell\ell$	eee	$ee\mu$	$e\mu\mu$	$\mu\mu\mu$
IH	27.07	10.297	16.314	0.459	0.0

heavy neutrinos for a benchmark mass of M_N at 100 GeV with the cuts discussed in Sec. IV A.

1. Signal for s-channel

The signal coming from the decay of heavy neutrinos

$$pp \to \ell^{\pm} N \to \ell^{\pm}(\ell^{\mp} W^{\pm}) \to \ell^{\pm}\ell^{\mp}\ell^{\pm} + \not{E}_T,$$

where $\ell \equiv \mathrm{e}, \mu$.

Table IV lists the final trilepton signal cross section through s-channel heavy neutrino production at 14 TeV LHC for the benchmark point $M_N = 100$ GeV incorporating all event selection criteria except VBF cuts as described earlier. The total contribution from the light leptons as well as the contributions from the four different flavor combinations are presented.

As we can see from the Table IV, the cross section in terms of flavors has the ordering: $ee\mu > eee > e\mu\mu > \mu\mu\mu$. We can understand this in the following way. There are a total of 8 possibilities which can produce $\ell\ell\ell$ events. There is only one way to produce $\mu\mu\mu$ and eee final states. However, there are three possible ways to get the $ee\mu$ channel depending on which one of ℓ_i's in Fig. 2 is associated with e and μ. Similarly for the $e\mu\mu$ final state also we get 3 possibilities. The amplitude for the eee channel $\sim V_{eN}^4$, the $ee\mu$ channel goes as $\sim V_{eN}^2 + 2V_{eN}V_{\mu N}$, the $e\mu\mu$ channel goes as $\sim V_{\mu N}^2 + 2V_{eN}V_{\mu N}$, while the $\mu\mu\mu$ channel goes as $\sim V_{\mu N}^2$. Since $V_{eN} \gg V_{\mu N}$, the eee and $ee\mu$ cross sections are much larger, whereas the $\mu\mu\mu$ cross section is negligible. The $ee\mu$ cross section is higher than the eee cross section because of higher muon efficiency in the detector, whereas the small $e\mu\mu$ cross section is due to a very tiny value of $V_{\mu N}$.

One can also compute the ratios of events with different flavor compositions in which some of the common systematic uncertainties can get canceled. For example $ee\mu/eee \sim \epsilon$ where ϵ denotes the relative efficiency of detection of the muon over the electron, $ee\mu/\mu\mu\mu \sim \epsilon V_{eN}^4/V_{\mu N}^4$, $eee/e\mu\mu \sim \epsilon^2 V_{eN}^4/V_{\mu N}^4$, etc. Since for a fixed y_ν, which in turn implies specific values for phases, the variation of the light-heavy mixing angles is not very much with oscillation parameters, these ratios vary within a very narrow range[9] and hence can be used to test the model. Of course, for different phase choices a different y_ν and hence different predictions can be obtained. However, a smaller value in y_ν would result in a lower event rate and hence it would be difficult to test at the LHC.

TABLE V. Final trilepton signal through VBF production of heavy neutrinos for the benchmark point $M_N = 100$ GeV at 14 TeV LHC for IH after all event selection cuts.

	Cross section (fb)				
Hierarchy	$\ell\ell\ell$	eee	$ee\mu$	$e\mu\mu$	$\mu\mu\mu$
IH	0.018068	7.09×10^{-3}	1.06×10^{-2}	4.06×10^{-4}	0.00

2. Signal for VBF

In this section we present the results for the case where N is produced by VBF:

$$pp \to \ell^{\pm} N jj \to \ell^{\pm}(\ell^{\mp} W^{\pm}) jj \to \ell^{\pm}\ell^{\mp}\ell^{\pm} + \not{E}_T + jj(\text{forward jets}), \quad \text{where } \ell \equiv \mathrm{e}, \mu.$$

In Table V we present the final trilepton signal cross sections through VBF production of heavy neutrinos at the 14 TeV LHC for the benchmark point $M_N = 100$ GeV, after including all cuts. Here we have only shown the case of inverted hierarchy and signal is found to be quite small. Although VBF backgrounds are small, the tiny production cross sections are insufficient for giving any signal with an integrated luminosity of 300 fb^{-1}. Some indications from VBF can appear only at the HL-LHC (3000 fb^{-1}). However, 5σ significance cannot be reached even for $M_N = 100$ GeV.

V. DISCOVERY POTENTIAL

After numerical computation of all necessary signals and backgrounds, results are better represented in terms of significance, defined as $S/\sqrt{S+B}$, where $S(B) = \mathcal{L}\sigma_{S(B)}$. Here, $\mathcal{L}$ is the integrated luminosity available for the collider at a certain machine energy and $\sigma_{S(B)}$ is the final cross section after all event selections, for given parameters like heavy neutrino mass and corresponding allowed couplings. Figure 6 (left) demonstrates the expected significance coming from the s-channel production of the heavy Dirac neutrino of mass 100 GeV as a function of

[9]Note that, the allowed magnitude of mixings are as following: For a fixed value of $y_\nu(= 0.4)$, $\alpha(= 3\pi/4)$, $\delta(= 0)$, and $M_N(= 100)$ GeV, the magnitude of $|V_{eN}|$ and $|V_{\mu N}|$ vary in a very small range for 3σ variation of oscillation parameters; $|V_{eN}| = 0.471$–0.484, $|V_{\mu N}| = 1.236 \times 10^{-4}$–$1.272 \times 10^{-4}$. However, $|V_{\tau N}|$ varies little higher; $|V_{\tau N}| = 0.092$–0.147. Since we are considering modes involving only e and μ, the cross sections are likely to vary by a small amount for different set of oscillation parameters.

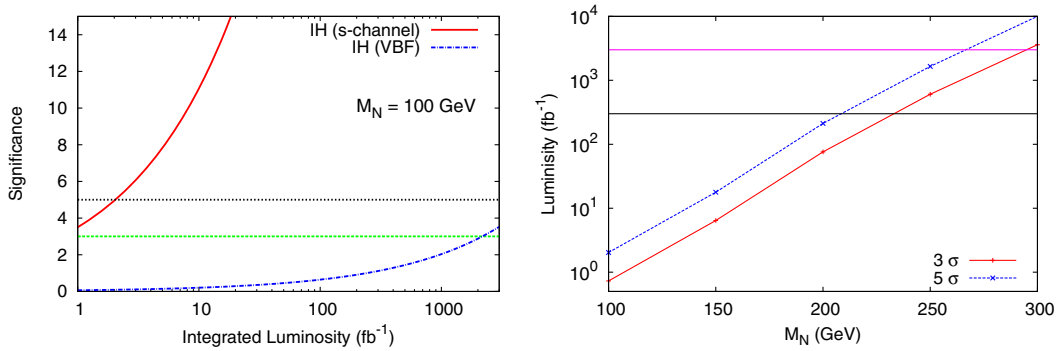

FIG. 6 (color online). (Left) The variation of significance $S/\sqrt{S+B}$ for the s-channel production signal for benchmark point $M_N = 100$ GeV with the integrated luminosity available for the low luminosity option at 14 TeV LHC. Black-dotted (green-dashed) line parallel to the x axis represents the 5σ (3σ) significance. (Right) The lines for the 3σ (red) and 5σ (blue) significance in terms of heavy neutrino mass and integrated luminosity. With 300 fb^{-1} luminosity at LHC14, the heavy neutrino mass in this model can be probed up to $\sim$210(230) GeV with $\sim 5\sigma$ (3σ) significance. For a very high luminosity of 3000 fb^{-1} this can reach up to $\sim$270(295) GeV.

integrated luminosity at 14 TeV LHC. In the figure, the black-dotted (green-dashed) line shows 5σ (3σ) significance. From the figure it is clear that for the case of the s-channel signal in the IH scenario, the 3σ (5σ) significance can be achieved within the integrated luminosity $\sim$0.73(2.03) fb^{-1}. In the case of the VBF channel 3σ significance can be achieved with 2175 fb^{-1} luminosity, while 5σ significance is not achievable within 3000 fb^{-1} luminosity which is planned for the HL-LHC.

Figure 6 (right) shows the lines for 3σ (red) and 5σ (blue) significance in terms of heavy neutrino mass and integrated luminosity. With 300 fb^{-1} luminosity at LHC14 the heavy neutrino mass in this model can be probed up to $\sim$210(230) GeV with $\sim 5\sigma$ (3σ) significance. For very high luminosity of 3000 fb^{-1} this can reach up to $\sim$270(295) GeV. For the VBF signal, since $M_N =$ 100 GeV, it requires a very large integrated luminosity; higher values of M_N are not possible to explore.

VI. SUMMARY AND CONCLUSION

In this work we have considered a TeV scale minimal linear seesaw model which generates the correct order of light neutrino masses and has sizable light-heavy mixing to produce heavy neutrinos at colliders like LHC. One of the important features of this model is that it can be fully reconstructible from oscillation data excepting an overall factor y_ν characterizing the Dirac Yukawa matrix. However, this parameter gets constrained by LFV and vacuum metastability bounds. The neutral fermion mass spectrum of this model consists of one massless, two light, and two heavy neutrinos.

We have studied the collider phenomenology of the TeV scale linear seesaw at 14 TeV LHC. The heavy neutrinos in this model can be dominantly produced through the s-channel. In a leading order calculation, subsequent decay of these leads to the characteristic trilepton signal with missing p_T. We also consider the production of heavy neutrinos through the VBF process. The signal for this is trileptons with additional two forward jets which can be tagged. Both these signals as well as the SM backgrounds have been estimated with realistic simulations using MadGraph and PYTHIA.

We found that s-channel trilepton production processes have the potential to be discovered at the LHC for the IH scenario. However, due to severe constraint on the light-heavy mixing coming from LFV in the case of the NH scenario, both the s-channel and VBF cannot be probed at the 14 TeV LHC with proposed luminosity. For a benchmark point with a heavy neutrino mass $M_N = 100$ GeV, 3σ significance can be achieved with an integrated luminosity of $\sim$0.73(2175) fb^{-1} for the s-channel (VBF) signal in the IH scenario. 5σ significance can be reached for the s-channel signal with an integrated luminosity of $\sim$2 fb^{-1}; however, for the VBF signal the required luminosity is $\sim$6042 fb^{-1}, which is beyond the reach of the projected luminosity at the LHC. The discovery reach in the trilepton channel can be achieved up to the heavy neutrino mass of $\sim$210(230) GeV with $\sim 5\sigma$ (3σ) significance at the low luminosity (300 fb^{-1}) option of 14 TeV LHC. In the high luminosity (3000 fb^{-1}) search, the reach is up to $\sim$270(295) GeV. Whereas, the VBF channel can only reach up to $\sim 3\sigma$ for M_N at 100 GeV. Our analysis uses values for the elements, V_{lN}, of the light-heavy mixing matrix, which are consistent with the constraints coming from vacuum metastability and LFV. Any freedom of choosing larger values [e.g. $\sim\mathcal{O}(1)$] for these parameters can extend the discovery limit by a very significant amount. With the constraints used in this work, for V_{lN}, a detectable trilepton signal can only be obtained for the inverted hierarchical scenario with particular choices of phases leading to large y_ν. One can also compute the ratios of events with different flavor compositions which are proportional to the elements V_{lN}. They vary only within a narrow range with the 3σ variations of oscillation parameters and thus the model has very definite predictions for these ratios.

[1] G. Aad *et al.* (ATLAS Collaboration), Phys. Lett. B **716**, 1 (2012).
[2] S. Chatrchyan *et al.* (CMS Collaboration), Phys. Lett. B **716**, 30 (2012).
[3] P. Ade *et al.* (Planck Collaboration), Astron. Astrophys. **571**, A16 (2014).
[4] S. Weinberg, Phys. Rev. Lett. **43**, 1566 (1979).
[5] P. Minkowski, Phys. Lett. **67B**, 421 (1977).
[6] T. Yanagida, Conf. Proc. **C7902131**, 95 (1979).
[7] M. Gell-Mann, P. Ramond, and R. Slansky, Conf. Proc. **C790927**, 315 (1979).
[8] S. Glashow, NATO Adv. Study Inst. Ser. B Phys. **59**, 687 (1980).
[9] R. N. Mohapatra and G. Senjanovic, Phys. Rev. Lett. **44**, 912 (1980).
[10] A. Pilaftsis, Z. Phys. C **55**, 275 (1992).
[11] J. Gluza, arXiv:hep-ph/0201002
[12] A. Pilaftsis, Phys. Rev. Lett. **95**, 081602 (2005).
[13] J. Kersten and A. Y. Smirnov, Phys. Rev. D **76**, 073005 (2007).
[14] Z.-z. Xing, Prog. Theor. Phys. Suppl. **180**, 112 (2009).
[15] X.-G. He, S. Oh, J. Tandean, and C.-C. Wen, Phys. Rev. D **80**, 073012 (2009).
[16] A. Ibarra, E. Molinaro, and S. Petcov, J. High Energy Phys. 09 (2010) 108.
[17] F. F. Deppisch and A. Pilaftsis, Phys. Rev. D **83**, 076007 (2011).
[18] R. Adhikari and A. Raychaudhuri, Phys. Rev. D **84**, 033002 (2011).
[19] I. Gogoladze, N. Okada, and Q. Shafi, Phys. Lett. B **672**, 235 (2009).
[20] K. Babu, S. Nandi, and Z. Tavartkiladze, Phys. Rev. D **80**, 071702 (2009).
[21] F. Bonnet, D. Hernandez, T. Ota, and W. Winter, J. High Energy Phys. 10 (2009) 076.
[22] S. Kanemura and T. Ota, Phys. Lett. B **694**, 233 (2010).
[23] Y. Liao, G.-Z. Ning, and L. Ren, Phys. Rev. D **82**, 113003 (2010).
[24] I. Picek and B. Radovcic, Phys. Lett. B **687**, 338 (2010).
[25] Y. Liao, J. High Energy Phys. 06 (2011) 098.
[26] K. Kumericki, I. Picek, and B. Radovcic, Phys. Rev. D **86**, 013006 (2012).
[27] K. L. McDonald, J. High Energy Phys. 07 (2013) 020.
[28] A. Zee, Phys. Lett. **93B**, 389 (1980).
[29] A. Zee, Nucl. Phys. **B264**, 99 (1986).
[30] K. Babu, Phys. Lett. **B203**, 132 (1988).
[31] L. M. Krauss, S. Nasri, and M. Trodden, Phys. Rev. D **67**, 085002 (2003).
[32] E. Ma, Phys. Rev. D **73**, 077301 (2006).
[33] M. Aoki, S. Kanemura, and O. Seto, Phys. Rev. Lett. **102**, 051805 (2009).
[34] P. B. Dev and A. Pilaftsis, Phys. Rev. D **86**, 113001 (2012).
[35] M. Gustafsson, J. M. No, and M. A. Rivera, Phys. Rev. D **90**, 013012 (2014).
[36] R. Mohapatra and J. Valle, Phys. Rev. D **34**, 1642 (1986).
[37] W.-Y. Keung and G. Senjanovic, Phys. Rev. Lett. **50**, 1427 (1983).
[38] A. Datta, M. Guchait, and A. Pilaftsis, Phys. Rev. D **50**, 3195 (1994).
[39] T. Han and B. Zhang, Phys. Rev. Lett. **97**, 171804 (2006).
[40] S. Bray, J. S. Lee, and A. Pilaftsis, Nucl. Phys. **B786**, 95 (2007).
[41] F. del Aguila, J. Aguilar-Saavedra, and R. Pittau, J. High Energy Phys. 10 (2007) 047.
[42] F. del Aguila and J. Aguilar-Saavedra, Nucl. Phys. **B813**, 22 (2009).
[43] A. Atre, T. Han, S. Pascoli, and B. Zhang, J. High Energy Phys. 05 (2009) 030.
[44] S. Chatrchyan *et al.* (CMS Collaboration), Phys. Lett. B **717**, 109 (2012).
[45] P. S. B. Dev, A. Pilaftsis, and U.-k. Yang, Phys. Rev. Lett. **112**, 081801 (2014).
[46] A. Das, P. B. Dev, and N. Okada, Phys. Lett. B **735**, 364 (2014).
[47] F. del Aguila and J. Aguilar-Saavedra, Phys. Lett. B **672**, 158 (2009).
[48] C.-Y. Chen and P. B. Dev, Phys. Rev. D **85**, 093018 (2012).
[49] A. Das and N. Okada, Phys. Rev. D **88**, 113001 (2013).
[50] O. Eboli, J. Gonzalez-Fraile, and M. Gonzalez-Garcia, J. High Energy Phys. 12 (2011) 009.
[51] S. Chatrchyan *et al.* (CMS Collaboration), Phys. Rev. D **90**, 032006 (2014).
[52] M. Gavela, T. Hambye, D. Hernandez, and P. Hernandez, J. High Energy Phys. 09 (2009) 038.
[53] S. Khan, S. Goswami, and S. Roy, Phys. Rev. D **89**, 073021 (2014).
[54] M. Malinsky, T. Ohlsson, Z.-z. Xing, and H. Zhang, Phys. Lett. B **679**, 242 (2009).
[55] D. L. Rainwater, arXiv:hep-ph/9908378.
[56] A. Datta, P. Konar, and B. Mukhopadhyaya, Phys. Rev. Lett. **88**, 181802 (2002).
[57] D. Choudhury, A. Datta, K. Huitu, P. Konar, S. Moretti, and B. Mukhopadhyaya, Phys. Rev. D **68**, 075007 (2003).
[58] G.-C. Cho, K. Hagiwara, J. Kanzaki, T. Plehn, D. Rainwater, and T. Stelzer, Phys. Rev. D **73**, 054002 (2006).
[59] P.-H. Gu and U. Sarkar, Phys. Lett. B **694**, 226 (2010).
[60] H. Zhang and S. Zhou, Phys. Lett. B **685**, 297 (2010).
[61] M. Hirsch, S. Morisi, and J. Valle, Phys. Lett. B **679**, 454 (2009).
[62] F. Bazzocchi, Phys. Rev. D **83**, 093009 (2011).
[63] W. Grimus and L. Lavoura, J. High Energy Phys. 11 (2000) 042.
[64] S. Khan, Nucl. Phys. **B864**, 38 (2012).
[65] J. de Blas, Europhys. J. Web Conf. **60**, 19008 (2013).
[66] G. Bozzi, B. Jager, C. Oleari, and D. Zeppenfeld, Phys. Rev. D **75**, 073004 (2007).
[67] B. Jager, C. Oleari, and D. Zeppenfeld, Phys. Rev. D **73**, 113006 (2006).
[68] J. Pumplin, D. Stump, J. Huston, H. Lai, P. M. Nadolsky, P. Nadolsky, and W-K. Tung, J. High Energy Phys. 07 (2002) 012.
[69] J. Eckel, M. J. Ramsey-Musolf, W. Shepherd, and S. Su, J. High Energy Phys. 11 (2014) 117.
[70] N. D. Christensen and C. Duhr, Comput. Phys. Commun. **180**, 1614 (2009).
[71] J. Alwall, M. Herquet, F. Maltoni, O. Mattelaer, and T. Stelzer, J. High Energy Phys. 06 (2011) 128.
[72] J. Alwall, A. Ballestrero, P. Bartalini, S. Belov, E. Boos *et al.*, Comput. Phys. Commun. **176**, 300 (2007).

[73] T. Sjostrand, S. Mrenna, and P. Z. Skands, J. High Energy Phys. 05 (2006) 026.
[74] G. Bambhaniya, J. Chakrabortty, S. Goswami, and P. Konar, Phys. Rev. D **88**, 075006 (2013).
[75] B. Mukhopadhyaya and S. Mukhopadhyay, Phys. Rev. D **82**, 031501 (2010).
[76] G. Aad *et al.* (ATLAS Collaboration), arXiv:0901.0512.
[77] G. Bayatian *et al.* (CMS Collaboration), J. Phys. D **34**, 995 (2007).
[78] E. Yazgan, J. Damgov, N. Akchurin, V. Genchev, D. Green, S. Kunori, M. Schmitt, W. Wu, and M. T. Zeyrek*et al.*, Eur. Phys. J. C **53**, 329 (2008).
[79] G. Bambhaniya, J. Chakrabortty, J. Gluza, M. Kordiaczynska, and R. Szafron, J. High Energy Phys. 05 (2014) 033.
[80] M. L. Mangano, M. Moretti, F. Piccinini, R. Pittau, and A. D. Polosa, J. High Energy Phys. 07 (2003) 001.